

Analysis of atmospheric effects on the continuous variable quantum key distribution

Tao Liu(刘涛), Shuo Zhao(赵硕), Ivan B. Djordjevic, Shuyu Liu(刘舒宇), Sijia Wang(王思佳),Tong Wu(吴彤), Bin Li(李斌), Pingping Wang(王平平), and Rongxiang Zhang(张荣香)

Citation: Chin. Phys. B, 2022, 31 (**11**): 110303. DOI: 10.1088/1674-1056/ac6b1f

What follows is a list of articles you may be interested in

Improvement of a continuous-variable measurement-device-independent quantum key distribution system via quantum scissors

Lingzhi Kong(孔令志), Weiqi Liu(刘维琪), Fan Jing(荆凡), Zhe-Kun Zhang(张哲坤), Jin Qi(齐锦), and Chen He(贺晨)

Chin. Phys. B, 2022, 31 (**9**): 090304. DOI: 10.1088/1674-1056/ac6dba

Probabilistic quantum teleportation of shared quantum secret

Hengji Li(李恒吉), Jian Li(李剑), and Xiubo Chen(陈秀波)

Chin. Phys. B, 2022, 31 (**9**): 090303. DOI: 10.1088/1674-1056/ac67c0

Direct measurement of two-qubit phononic entangled states via optomechanical interactions

A-Peng Liu(刘阿鹏), Liu-Yong Cheng(程留永), Qi Guo(郭奇), Shi-Lei Su(苏石磊), Hong-Fu Wang(王洪福), and Shou Zhang(张寿)

Chin. Phys. B, 2022, 31 (**8**): 080307. DOI: 10.1088/1674-1056/ac5d2f

Purification in entanglement distribution with deep quantum neural network

Jin Xu(徐瑾), Xiaoguang Chen(陈晓光), Rong Zhang(张蓉), and Hanwei Xiao(肖晗微)

Chin. Phys. B, 2022, 31 (**8**): 080304. DOI: 10.1088/1674-1056/ac6330

Finite-key analysis of practical time-bin high-dimensional quantum key distribution with afterpulse effect

Yu Zhou(周雨), Chun Zhou(周淳), Yang Wang(汪洋), Yi-Fei Lu(陆宜飞), Mu-Sheng Jiang(江木生), Xiao-Xu Zhang(张晓旭), and Wan-Su Bao(鲍皖苏)

Chin. Phys. B, 2022, 31 (**8**): 080303. DOI: 10.1088/1674-1056/ac6017

Analysis of atmospheric effects on the continuous variable quantum key distribution

Tao Liu(刘涛)[1,2,3,†], Shuo Zhao(赵硕)[1], Ivan B. Djordjevic[4], Shuyu Liu(刘舒宇)[1], Sijia Wang(王思佳)[1], Tong Wu(吴彤)[1], Bin Li(李斌)[1], Pingping Wang(王平平)[1], and Rongxiang Zhang(张荣香)[5]

[1] *Department of Electronic and Communication Engineering, North China Electric Power University, Baoding* 071003, *China*
[2] *Hebei Key Laboratory of Power Internet of Things Technology, North China Electric Power University, Baoding* 071003, *China*
[3] *Baoding Key Laboratory of Optical Fiber Sensing and Optical Communication Technology, North China Electric Power University, Baoding* 071003, *China*
[4] *Department of Electrical and Computer Engineering, University of Arizona,* 1230 *E Speedway Blvd., Tucson, Arizona* 85721, *USA*
[5] *College of Physics Science and Technology, Hebei University, Baoding* 071002, *China*

(Received 3 January 2022; revised manuscript received 10 April 2022; accepted manuscript online 28 April 2022)

Atmospheric effects have significant influence on the performance of a free-space optical continuous variable quantum key distribution (CVQKD) system. In this paper, we investigate how the transmittance, excess noise and interruption probability caused by atmospheric effects affect the secret-key rate (SKR) of the CVQKD. Three signal wavelengths, two weather conditions, two detection schemes, and two types of attacks are considered in our investigation. An expression aims at calculating the interruption probability is proposed based on the Kolmogorov spectrum model. The results show that a signal using long working wavelength can propagate much further than that of using short wavelength. Moreover, as the wavelength increases, the influence of interruption probability on the SKR becomes more significant, especially within a certain transmission distance. Therefore, interruption probability must be considered for CVQKD by using long-signal wavelengths. Furthermore, different detection schemes used by the receiver will result in different transmission distances when subjected to individual attacks and collective attacks, respectively.

Keywords: atmospheric effect, continuous variable key distribution, free space quantum communication, secret-key rate

PACS: 03.67.Hk, 42.68.Bz **DOI:** 10.1088/1674-1056/ac6b1f

1. Introduction

Quantum communication in free-space optical (FSO) channels has recently attracted much attention due to the low-transmission loss and flexible installation.[1] It has become an important way to realize a global quantum communication network.[2] However, when the optical beam propagates over the atmosphere, it is inevitably affected by atmospheric effects such as absorption, scattering, and turbulence. Turbulence caused by atmospheric motion and heating is the main factor affecting the performance of the FSO quantum communication system. It can lead to random fluctuation of the atmospheric refractive index, which can cause light intensity flickering, beam drift, angle-of-arrival fluctuations, phase fluctuations, and beam expansion. All of these natural but troublesome atmospheric occurrences affect optical signals as they propagate through the atmosphere. Communication may even be interrupted due to the transmittance change,[3,4] in particular in strong turbulence regime.

The theory of classical light transmission through the atmosphere is well developed.[5–7] Some progress in the theory of free space transmission of quantum light is also obtained. Vasylyev *et al.*[8] derived the consistent probability distribution of transmittance for three channel models of the beam wandering model, elliptical beam model, and the model with the law of total probability by step-by-step inclusion of various atmospheric effects such as beam wandering, beam broadening and deformation of the beam into elliptic form, beam deformations into arbitrary forms. Chai *et al.*[9] investigated the atmospheric effects on the excess noise in FSO continuous variable quantum key distribution (CVQKD) and analyzed the excess noise tolerance of systems with diverse modulations, which provided a certain theoretical basis for studying the effect of excess noise on the performance of secret-key rate (SKR). Zhao *et al.*[10] investigated intensity scintillation effects, atmospheric transmittance, and phase noise caused by atmospheric turbulence on communication performance in the satellite-to-ground CVQKD system-based orthogonal frequency division multiplexing system. These studies[8–10] carefully investigated the influence of atmospheric turbulence on communication performance, but they did not cover the impact of interruption probability on the quantum communication performance, which is also caused by atmospheric turbulence. Wang *et al.*[11] considered the interruption probability in their study of the effects of atmospheric scattering and turbulence on CVQKD SKR. However, even though they determined the interruption probability to have an impact on the

[†]Corresponding author. E-mail: taoliu@ncepu.edu.cn
© 2022 Chinese Physical Society and IOP Publishing Ltd

SKR, the corresponding analysis was not carried out. Besides, the studies so far considered only a single wavelength for transmission. It is well known that, for the classical laser FSO communication system, signals with different wavelengths get differently affected by the atmospheric effects.[12] Thus, it is necessary to investigate the atmospheric effects on the FSO CVQKD system identify the most suitable wavelength showing better tolerance to various atmospheric effects. Also, for the classical laser FSO communication system, several spectrum models, including the Kolmogorov spectrum model, the von Kármán spectrum model, and the modified von Kármán spectrum model, can be used to theoretically investigate the effect of turbulence on optical signals.[13] Compared to the von Kármán spectrum model and modified von Kármán spectrum model, the Kolmogorov spectrum model is simple thus it is more widely used. However, research is difficult to find on the effect of atmospheric turbulence on the performance of FSO quantum communication system by using the Kolmogorov spectrum model.[11,14]

From the reported studies[15–17] one can see that, the wavelengths around 810 nm are widely used in the satellite-to-ground quantum communication systems, the 1550 nm can be utilized to overcome the background noise due to sunlight in daylight, and the 3800 nm wavelength has the advantage of being affected less by atmospheric effects compared to the 810 nm and 1550 nm wavelengths. Therefore, in this paper, the three wavelengths (810 nm, 1550 nm, and 3800 nm) are used in the investigation of atmospheric effects on the FSO CVQKD system with the goal to identify the wavelength region more tolerant to various atmospheric effects. Two weather conditions, homodyne and heterodyne detection cases, and individual and collective attacks are considered in our study. A CVQKD model for transmission over free-space optical channel is established firstly and then it is used to analyze the simultaneous effects of transmittance, excess noise and interruption probability on the SKR of the CVQKD. A formula to calculate the interruption probability is achieved based on the Kolmogorov spectrum model and used in the simulation. In clear weather, the results show that, the SKR decreases with the increase of transmission distance for all three wavelengths, but the transmission distance at 3800 nm is much larger than that of 810 nm and 1550 nm at the same SKR. With the increase of wavelength, the effect of interruption probability on the SKR becomes more significant especially within a certain range of transmission distance, such as at the range of 10 km–100 km for 3800 nm wavelength. Thus, this effect must be considered for CVQKD by using long-signal wavelength. Moreover, to achieve longer transmission distance, the receiver should use homodyne detection in case of collective attacks, whereas heterodyne detection is recommended if the CVQKD system is under individual attacks. Similar results are obtained in fog except that the transmission distance is much shorter than that found in clear weather.

2. Free-space optical CVQKD transmission model

The FSO CVQKD system is a flexible system that can be easy installed and repositioned compared to the fiber-based solution, but affected by atmospheric effects, so it is essential to investigate the effects of atmosphere on the SKR. An entanglement-based CVQKD model with Gaussian modulation is observed and illustrated in Fig. 1. The sender (Alice) and receiver (Bob) share a pair of two-mode squeezed entangled states generated by the Einstein–Podolsky–Rosen (EPR) entangled source with variance V. One mode of the entangled state A is measured by Alice using homodyne detection, where $x_{\rm A}$ and $p_{\rm A}$ are the quadratures of the entangled state A, respectively. Meanwhile, another entangled state B_0, which is transmitted to Bob through an atmospheric channel with a transmittance T and excess noise ε, becomes mode B_1 after transmission. The channel extra noise observed from the channel input point of view is given by $\chi_{\rm line} = 1/T - 1 + \varepsilon$.

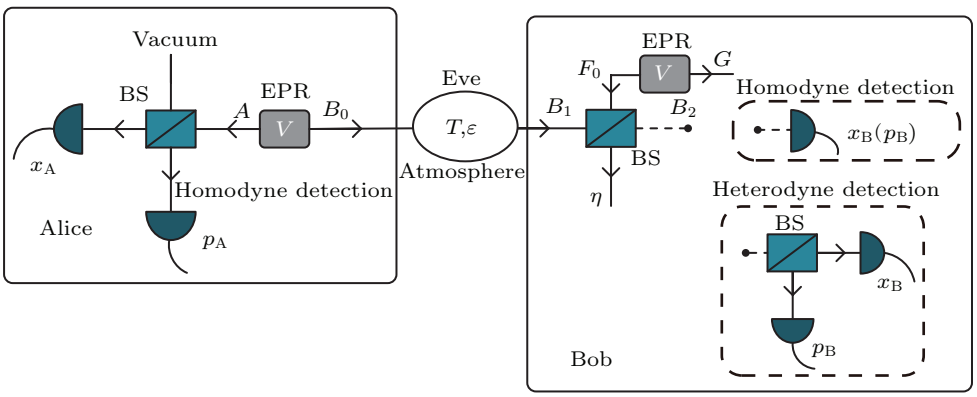


Fig. 1. Entanglement-based CVQKD model. BS, beam splitter.

Bob's detector efficiency is modeled by a beam splitter with transmission η, while its electronic noise $v_{\rm el}$ is modeled by an EPR state of variance v. As shown in Fig. 1, the F_0 mode is coupled into the second input port of the beam splitter. v is given by $v_{\rm hom}=\eta\chi_{\rm hom}/(1-\eta)$ and $v_{\rm het}=(\eta\chi_{\rm het}-1)/(1-\eta)$ for homodyne and heterodyne detection, respectively, where $\chi_{\rm hom}=((1-\eta)+v_{\rm el})/\eta$ and $\chi_{\rm het}=(1+(1-\eta)+2v_{\rm el})/\eta$ are the total noise of the actual homodyne and heterodyne detection, respectively. When the communication is completed, Alice and Bob perform classical data processing to obtain the final, secure quantum key through processes such as information reconciliation and privacy amplification.

Assuming that Alice and Bob adopt the reverse reconciliation approach, the SKR of the free-space CVQKD system with Gaussian modulation in the case of individual attacks and collective attacks is calculated as follows.

(1) The secret key rate for the case of collective attacks is given by[11]

$$K_{\rm atm}=(1-P)\left(\beta I_{\rm AB}-\chi_{\rm BE}\right), \tag{1}$$

where P is the probability of communication interruption, β is the reconciliation efficiency, $I_{\rm AB}$ is the Shannon mutual information of Alice and Bob, and $\chi_{\rm BE}$ indicates the upper limit of the amount of information Eve can obtain from Bob,[18,19] which can be expressed as

$$\chi_{\rm BE}=\sum_{i=1}^{2}G\left(\frac{\lambda_i-1}{2}\right)-\sum_{i=3}^{5}G\left(\frac{\lambda_i-1}{2}\right), \tag{2}$$

where $G(x)=(x+1)\log_2(x+1)-x\log_2(x)$ with λ_i being the i-th symplectic eigenvalue of the covariance matrix of the quantum system. The symplectic eigenvalues $\lambda_{1,2}$ can be calculated for both homodyne and heterodyne detection by[20]

$$\lambda_{1,2}^2=\frac{1}{2}\left(A\pm\sqrt{A^2-4B}\right) \tag{3}$$

with $A=V^2(1-2T)+2T+T^2(V+\chi_{\rm line})^2$ and $B=T^2(V\chi_{\rm line}+1)^2$. The symplectic eigenvalues $\lambda_{3,4}$ can take the same form as

$$\lambda_{3,4}^2=\frac{1}{2}\left(C\pm\sqrt{C^2-4D}\right) \tag{4}$$

for both the homodyne and heterodyne cases, while λ_5 is found to be 1. The C and D in Eq. (4) are defined as

$$C_{\rm hom}=\frac{A\chi_{\rm hom}+V\sqrt{B}+T(V+\chi_{\rm line})}{T\left(V+\chi_{\rm tot}^{\rm hom}\right)}, \tag{5}$$

$$D_{\rm hom}=\sqrt{B}\frac{V+\sqrt{B}\chi_{\rm hom}}{T\left(V+\chi_{\rm tot}^{\rm hom}\right)} \tag{6}$$

for homodyne detection and

$$C_{\rm het}=\frac{1}{\left[T\left(V+\chi_{\rm tot}^{\rm het}\right)\right]^2}\{A\chi_{\rm het}^2+B+1+2\chi_{\rm het}\left[V\sqrt{B}+T(V+\chi_{\rm time})\right]+2T\left(V^2-1\right)\}, \tag{7}$$

$$D_{\rm het}=\left[\frac{V+\sqrt{B}\chi_{\rm het}}{T\left(V+\chi_{\rm tot}^{\rm het}\right)}\right]^2 \tag{8}$$

for the heterodyne detection.

We can get the mutual information on Alice and Bob for homodyne detection[21–23]

$$I_{\rm AB}^{\rm hom}=\frac{1}{2}\log_2\left(\frac{V+\chi_{\rm tot}^{\rm hom}}{1+\chi_{\rm tot}^{\rm hom}}\right), \tag{9}$$

where $\chi_{\rm tot}^{\rm hom}$ is the total noise defined as $\chi_{\rm tot}^{\rm hom}=\chi_{\rm line}+\chi_{\rm hom}/T$. For heterodyne detection, the mutual information of Alice and Bob has a similar expression as that of the homodyne case, which is given by

$$I_{\rm AB}^{\rm het}=\log_2\left(\frac{V+\chi_{\rm tot}^{\rm het}}{1+\chi_{\rm tot}^{\rm het}}\right), \tag{10}$$

where the total noise $\chi_{\rm tot}^{\rm het}=\chi_{\rm line}+\chi_{\rm het}/T$.

(2) The secret key rate for the case of individual attacks is expressed as

$$K_{\rm atm}=(1-P)\left(\beta I_{\rm AB}-I_{\rm BE}\right), \tag{11}$$

where $I_{\rm AB}$ has the same expressions as Eqs. (9) and (10) for homodyne and heterodyne detections, respectively.

The $I_{\rm BE}$ is the maximum information on Bob's key available to Eve and is limited by the Shannon bound, which can be calculated by[21]

$$I_{\rm BE}^{\rm hom}=\frac{1}{2}\log_2\frac{T^2\left(V+\chi_{\rm tot}^{\rm hom}\right)\left(1/V+\chi_{\rm line}\right)}{1+T\chi_{\rm hom}\left(1/V+\chi_{\rm line}\right)} \tag{12}$$

for homodyne detection and

$$I_{\rm BE}^{\rm het}=\log_2\left[\frac{T\left(V+\chi_{\rm tot}^{\rm het}\right)\left(V+x_{\rm E}\right)}{Vx_{\rm E}+1+\chi_{\rm het}\left(V+x_{\rm E}\right)}\right] \tag{13}$$

for heterodyne detection, where

$$x_{\rm E}=\frac{T(2-\varepsilon)^2}{\left(\sqrt{2-2T+T\varepsilon}+\sqrt{\varepsilon}\right)^2}+1. \tag{14}$$

It can be seen from Eqs. (1) and (9) that the SKR of the free-space CVQKD system is related to the interruption probability P, the reconciliation efficiency β, the Shannon mutual information between Alice and Bob $I_{\rm AB}$, and the upper limit of the amount of information Eve obtained from Bob, which is denoted as $\chi_{\rm BE}$ and $I_{\rm BE}$ for collective and individual attacks, respectively. P is dominated by the fluctuation of the beam arrival angle due to the atmospheric turbulence, which can be reduced by the employment of the beam tracking system. In addition, $I_{\rm AB}$ varies with the transmittance T which is determined by the absorption and scattering of the molecules and aerosol in the atmosphere, and with the excess noise ε caused by the

pulse arrival time fluctuation because of the atmospheric turbulence. Since the atmospheric effects have a significant influence on the SKR, the next section will present a detailed analysis to help clarify the causes of the effects. In addition because the atmospheric effects are wavelength-dependent and affect the transmission distance, the signal wavelength and transmission distance are set as two main variables in the analysis.

3. Atmospheric effects on free-space optical CVQKD system

3.1. Transmittance

Transmittance fluctuations can cause beam wandering, broadening, deformation, and scintillation, which will have a certain impact on the SKR. For horizontal path, the transmittance is given by[24]

$$T_{\text{ext}}(L) = \mathrm{e}^{-\alpha(\lambda)L}, \tag{15}$$

where $\alpha(\lambda) = \alpha_{\text{sca}}^{\text{aer}}(\lambda) + \alpha_{\text{abs}}^{\text{aer}}(\lambda) + \alpha_{\text{sca}}^{\text{mol}}(\lambda) + \alpha_{\text{abs}}^{\text{mol}}(\lambda)$ is the total extinction coefficient. $\alpha_{\text{sca}}^{\text{aer}}(\lambda)$, $\alpha_{\text{abs}}^{\text{aer}}(\lambda)$, $\alpha_{\text{sca}}^{\text{mol}}(\lambda)$, and $\alpha_{\text{abs}}^{\text{mol}}(\lambda)$ are aerosol scattering, aerosol absorption, molecular scattering, and molecular absorption, respectively.

In this paper, three different wavelengths of 810 nm, 1550 nm and 3800 nm are chosen to study the atmospheric effects on SKR to select the wavelength region more tolerant to turbulence effects. Because all the wavelengths are within the atmospheric transmission windows, the contribution of absorption to $\alpha(\lambda)$ is extremely small. For that reason, Mie scattering dominates the total extinction coefficient which can be calculated by[25]

$$\alpha(\lambda) = \left(\frac{3.91}{V_{\text{V}}}\right)\left(\frac{0.55}{\lambda}\right)^{q}, \tag{16}$$

where V_{V} is the atmospheric visibility, and q is the size distribution of the scattering particles given by

$$q = \begin{cases} 1.6 & (V_{\text{V}} > 50\ \text{km}), \\ 1.3 & (6\ \text{km} < V_{\text{V}} < 50\ \text{km}), \\ 0.16V_{\text{V}} + 0.34 & (1\ \text{km} < V_{\text{V}} < 6\ \text{km}), \\ V_{\text{V}} - 0.5 & (0.5\ \text{km} < V_{\text{V}} < 1\ \text{km}), \\ 0 & (V_{\text{V}} < 0.5\ \text{km}). \end{cases} \tag{17}$$

To simplify calculation, $\alpha(\lambda)$ is converted into the attenuation coefficient in dB/km expressed as

$$\alpha_{\text{spec}} = 10\lg(e)\,\alpha(\lambda). \tag{18}$$

It can be seen from Eq. (15) that the atmospheric transmittance is related to the atmospheric attenuation coefficient. The relationship between the attenuation coefficient and visibility for different signal wavelengths is shown in Fig. 2.

Figure 2 shows that the attenuation coefficient of the long-wavelength signal is smaller than that of the shorter-wavelengths for the same visibility. Take visibility of 23 km and 4 km for example, which denote the clear weather and fog respectively, the corresponding attenuation coefficients are 0.06 dB/km and 0.64 dB/km for 3800 nm wavelength, whereas those for 810 nm wavelength are 0.45 dB/km and 2.92 dB/km. Therefore, it is better to use longer wavelengths from attenuation point of view.

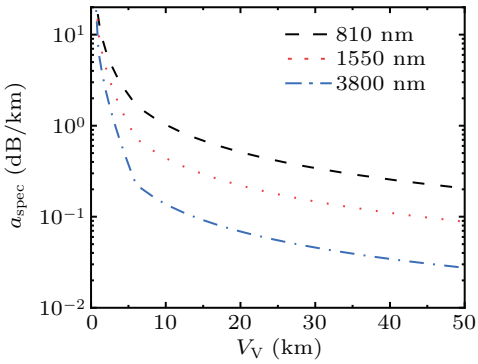


Fig. 2. The atmospheric attenuation as a function of the visibility for different wavelengths.

3.2. Excess noise

The optical pulse is affected by the atmosphere in the time domain, causing the pulse arrival time fluctuation, which further leads to the phase fluctuation. This effect may bring excess noise to the CVQKD system. As noted in the preceding section's analysis, the excess noise will affect the SKR. When the phase fluctuation is small enough, excess noise can be expressed as[26]

$$\varepsilon = V_{\text{A}}\sigma_{\theta}^{2}, \tag{19}$$

where V_{A} is the modulation variance of Alice, and σ_{θ}^{2} is the variance of phase fluctuation given by

$$\sigma_{\theta}^{2} = 2\omega^{2}(1-\rho_{\text{ta}})\,\sigma_{\text{ta}}^{2}, \tag{20}$$

where $\omega = 2\pi/\lambda$ is the angular frequency of the light, and ρ_{ta} is the correlation coefficient.[11] Under weak turbulence, $\sigma_{\text{ta}}^{2} = T_{1}^{2}/4$ is the on-axis variance of arrival time. The quantity $T_1 = \sqrt{T_0^2 + 8a_1}$ can be considered as the estimation of the broadened half-width at the receiver where T_0 is the input pulse half-width and $a_1 = 0.39C_n^2 L L_0^{5/3} c^{-2}$. C_n^2 is the refractive index structure parameter, which is constant for the horizontal paths. L is distance. L_0 is outer scale of atmosphere, and c is the speed of light.

It can be found from Eq. (19) that, the excess noise is a function of height, distance and signal wavelength. Under weak turbulence conditions, we consider $\rho_{\text{ta}} = 1 - 2\times10^{-14}$, $V_{\text{A}} = 10$ and $T_0 = 5\times10^{-8}$ s. The variation of excess noise varies with the height and distance at different wavelengths is summarized in Fig. 3. One can see from Fig. 3 that, under the same condition, excess noise at 810 nm, 1550 nm and 3800 nm wavelengths are about 0.15, 0.04 and 6.83×10^{-3}

(expressed in shot noise unit, SNU), respectively. The excess noise of 3800 nm is two orders of magnitude lower than that of 810 nm. That is, much higher SKR can be achieved by using the 3800 nm wavelength compared to the 810 nm wavelength.

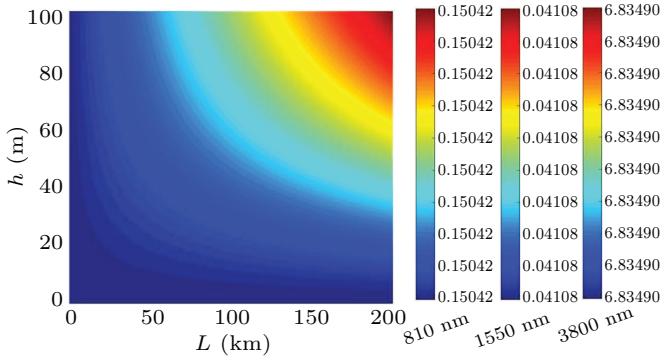


Fig. 3. Excess noise caused by phase fluctuation for different wavelengths.

3.3. Interruption probability

Atmospheric turbulence can lead to the fluctuation of a beam arrival angle, which can give rise to random jitter of the spot formed on the focal plane. When the angle of arrival fluctuation is too large, the spot on the focal plane cannot be in the receiving aperture, which will lead to communication interruption (see Fig. 4).

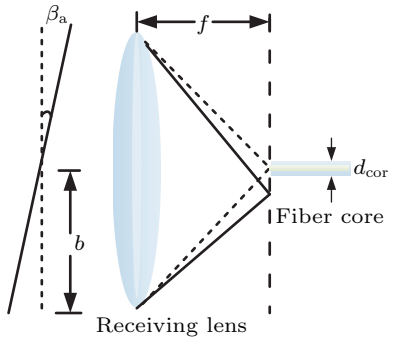


Fig. 4. Communication interruption due to the angle of arriving fluctuations.

The root mean square displacement of the lens can be calculated by

$$L_{dis} = f\sqrt{\langle \beta_a^2 \rangle}, \tag{21}$$

where f is the focal length of the lens.

From an optical point of view, the variance of the angle of arrival fluctuations is defined as[5]

$$\langle \beta_a^2 \rangle = \frac{D(2b,L)}{(2kb)^2}, \tag{22}$$

where $D(2b,L)$ is the phase structure function, b is the radius of the receiving lens, $k = 2\pi/\lambda$ is the optical wave number, and λ is light wavelength.

Here $\langle \beta_a^2 \rangle$ and L_{dis} are both assumed to obey normal distribution, and thus, the probability of communication interruption can be expressed as

$$P = 1 - \int_{-d_{cor}/2}^{d_{cor}/2} \frac{1}{\sqrt{2\pi f^2 \langle \beta_a^2 \rangle}} \exp\left(\frac{-l^2}{2f^2 \langle \beta_a^2 \rangle}\right) \mathrm{d}l, \tag{23}$$

where d_{cor} is the diameter of the fiber aperture.

It can be seen from Eqs. (22) and (23) that the interruption probability P is related to the transmission distance, the signal wavelength, and the phase structure function of atmospheric turbulence. For the Kolmogorov spectrum model, which is widely used in the simulation of turbulence, the phase structure function used to calculate P is derived as following.

The Kolmogorov spectrum is expressed as

$$\Phi_n(k) = 0.033 C_n^2 \kappa^{-11/3}. \tag{24}$$

The phase structure function $D(2b,L)$ based on the Kolmogorov spectrum model is

$$\begin{aligned} D(2b,L) = {} & 8\pi^2 k^2 L \int_0^1 \int_0^\infty \kappa \Phi_n(\kappa) \exp\left(\frac{-\Lambda L \kappa^2 \xi^2}{k}\right) \\ & \times \left\{ I_0(2\Lambda b \xi \kappa) - J_0\left[2\left(1-\bar{\Theta}\xi\right)\kappa b\right] \right\} \mathrm{d}\kappa \mathrm{d}\xi, \end{aligned} \tag{25}$$

where $\bar{\Theta} = -L/F$ and $\Lambda = 2L/kW^2$ are the non-dimensional output plane beam parameters. $F = L\left(1+\pi W_0^2/\lambda L\right)$ is the front curvature radius. W_0 is the beam radius of the emitter. The receiving end beam radius W can be calculated by

$$W = W_0\sqrt{1+\left(\lambda L/\pi W_0^2\right)^2}. \tag{26}$$

We simplify $D(2b,L)$ and divide it into two parts

$$D(2b,L) = d(2b,L) + 4\sigma_r^2(b,L), \tag{27}$$

where

$$\begin{aligned} d(2b,L) = {} & 8\pi^2 k^2 L \int_0^1 \int_0^\infty \kappa \Phi_n(\kappa) \exp\left(\frac{-\Lambda L \kappa^2 \xi^2}{k}\right) \\ & \times \left\{ 1 - J_0\left[2\left(1-\bar{\Theta}\xi\right)\kappa b\right] \right\} \mathrm{d}\kappa \mathrm{d}\xi \end{aligned} \tag{28}$$

with

$$\begin{aligned} \sigma_r^2(b,L) = {} & 2\pi^2 k^2 L \int_0^1 \int_0^\infty \kappa \Phi_n(\kappa) \exp\left(\frac{-\Lambda L \kappa^2 \xi^2}{k}\right) \\ & \times \left[I_0(2\Lambda b \xi \kappa) - 1 \right] \mathrm{d}\kappa \mathrm{d}\xi. \end{aligned} \tag{29}$$

Thus, Eq. (28) can be expressed in terms of confluent hypergeometric function ${}_1\mathrm{F}_1$ by

$$\begin{aligned} d(2b,L) = {} & 8.71 C_n^2 k^{7/6} L^{11/6} \Lambda^{5/6} \int_0^1 \xi^{5/3} \\ & \times \left\{ {}_1\mathrm{F}_1\left[-\frac{5}{6}; 1; -\frac{-\left(1-\bar{\Theta}\xi\right)^2 R^2}{4\Lambda\xi^2}\right] - 1 \right\} \mathrm{d}\xi, \end{aligned} \tag{30}$$

where $R^2 = 4kb^2/L$.

Equation (29) can also be expressed in terms of confluent hypergeometric function ${}_1\mathrm{F}_1$ by

$$\sigma_r^2(b,L) = 0.816 C_n^2 k^{7/6} L^{11/6} \Lambda^{5/6}$$

$$\times \left[1 - {}_1\mathrm{F}_1\left(-\frac{5}{6}; 1; \frac{2b^2}{W^2}\right)\right]. \quad (31)$$

Based on the Kolmogorov spectrum model, the interruption probability P is simulated as a function of distance in Fig. 5 for different wavelengths. Figure 5 shows that P for 810 nm, 1550 nm and 3800 nm wavelengths is a monotonically increasing function of the distance. Although P for short-wavelength at 810 nm is smaller than that of long-wavelength at 3800 nm, the difference between them is rather small. Especially in the range of transmission distance is less than 60 km, P of these two wavelengths are almost the same. Nevertheless, when the transmission distance exceeds 60 km, the difference of P between the two wavelengths will increase gradually as distance increases. In that case, if we only consider the influence of interruption probability on SKR, the shorter wavelengths are preferable. However, if the transmittance and excess noise are also considered, the short wavelength may not be the optimal choice. Therefore, it is necessary to comprehensively analyze the effect of different wavelengths on the performance of the FSO quantum communication system.

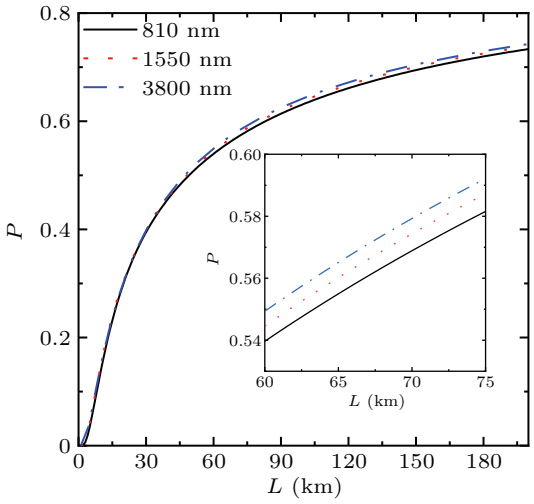


Fig. 5. The communication interruption probability varies depending on the distance capability of the different wavelengths.

4. Illustrative SKR results and discussion

In this section, the effects of the interruption probability P, transmittance T, and excess noise ε on the CVQKD system are analyzed. Different weather conditions, such as clear weather and fog, are considered in our investigation. Based on the above CVQKD model, in case of individual attacks and collective attacks, the SKRs for different signal wavelengths are calculated when Bob uses homodyne detection and heterodyne detection, respectively. The parameters used in the simulation are summarized in Table 1.

For homodyne detection, as shown from Fig. 6 the setup and operational mode must follow certain guidelines. The following is a summary of our analyzes.

Table 1. The parameters setting of SKR analysis with different wavelengths.

Character	Parameters	Values
λ	laser wavelength	810 nm, 1550 nm, and 3800 nm
d_{cor}	fiber core diameter	9 μm
W_0	transmitting lens radius	80 mm
b	receiving lens radius	110 mm
v_{el}	electronic noise	0.01 SUN
V_{A}	modulation variance	10 SUN
β	reconciliation efficiency	90%
η	detection efficiency	60%
V_{V1}	visibility in clear weather	23 km
V_{V2}	visibility in fog	4 km

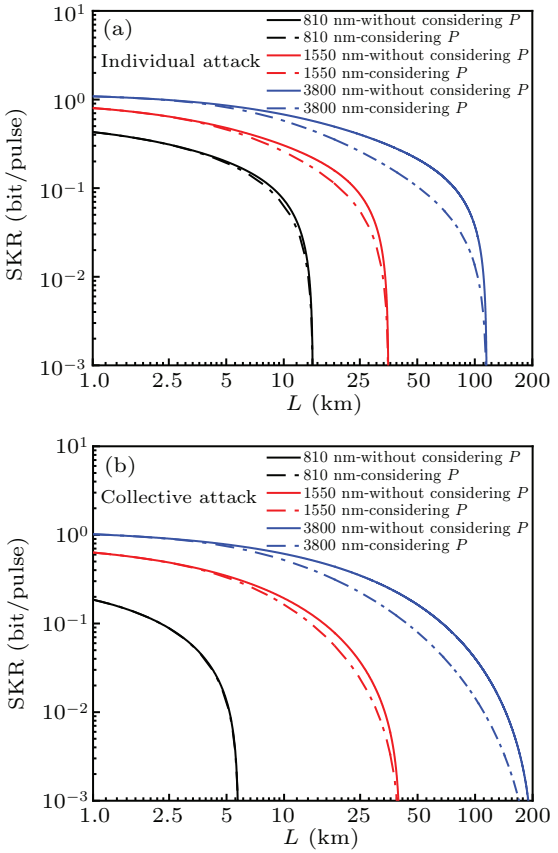


Fig. 6. Relationship between SKR and distance in case of (a) individual attacks and (b) collective attacks for homodyne detection in clear weather.

(1) In the case of individual attacks and collective attacks, all the SKRs for different signal wavelengths are monotonically decreasing functions of the transmission distance, as expected. However, compared to 810 nm wavelength region, which is widely used in the satellite-to-ground quantum communication systems,[27,28] and 1550 nm which is utilized to overcome the background noise due to sunlight in daylight,[16] the 3800 nm-based CVQKD has the longest propagation distance at the same SKR. For example, in case of individual attacks, when the SKR is 10^{-3} bit/channel use, the propagation distance of the 3800 nm wavelength signal is 115 km, which is 100 km and 80 km longer than that of 810 nm and 1550 nm, respectively. While under collective attacks, the propagation distance of 3800 nm reaches 190 km, which is 184 km and 150 km longer than that of 810 nm and 1550 nm, respectively.

Based on the results shown in Section 3, the signal with a long wavelength has a smaller excess noise ε, and much larger transmittance T in comparison with those of the shorter wavelengths signals. Though the interruption probability P of the former is higher than that of the latter, the difference between them is rather small. For this reason, a 3800 nm wavelength signal propagates at much longer distances compared to the 810 nm and 1550 nm wavelengths.

(2) The effect of interruption probability P on the SKR for different wavelengths is different. For example, with and without considering P, the SKRs of 810 nm are almost same. Thus, it is reasonable to neglect the influence of P in the simulation when we use a short wavelength signal. This is done to maintain a simplicity that is both efficient and easy to work with. However, when wavelengths increase, the P effect needs to be considered. Consider a 3800 nm wavelength as an example. Figure 6 clearly shows that not considering P does not provide the realistic estimate of the achievable transmission distance for a given SKR. To overcome this problem the beam tracking is necessary.

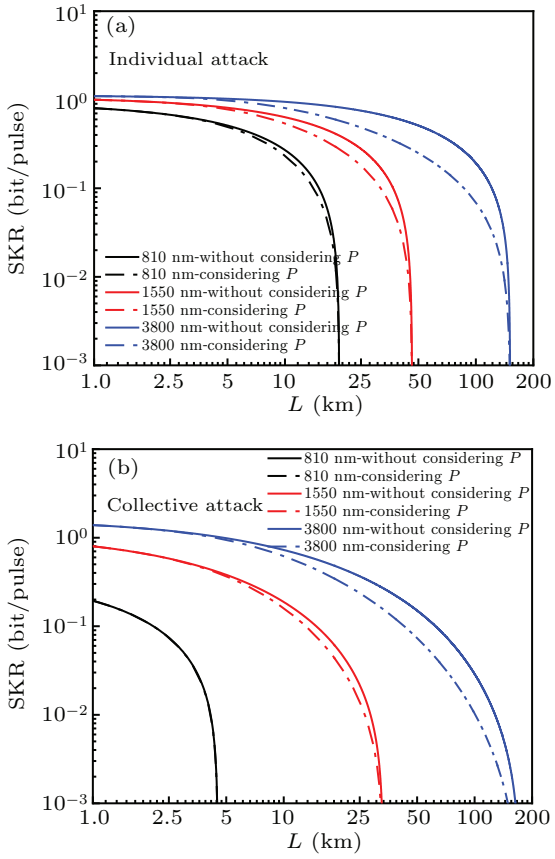


Fig. 7. Relationship between SKR and distance in case of (a) individual attacks and (b) collective attacks for heterodyne detection in clear weather.

In the case of heterodyne detection, someone may notice that the trends are the as that of homodyne detection. As illustrated in Fig. 7, the SKRs for different wavelengths also monotonically decreasing functions of transmission distance. Similarly, much longer transmission distance can be achieved at 3800 nm compared to the short wavelengths at the same SKR. The effects of interruption probability P, transmittance T, and excess noise εon the SKR for heterodyne detection are also similar to those of homodyne detection.

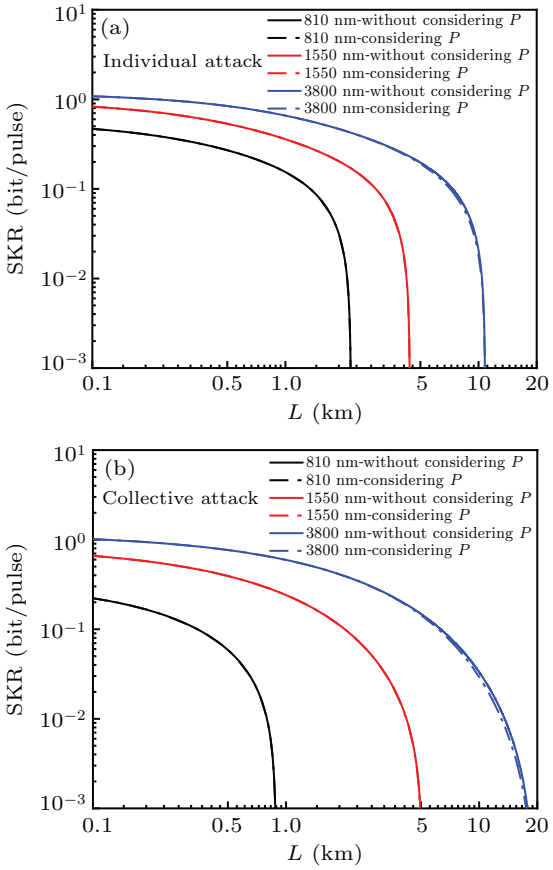


Fig. 8. Relationship between SKR and distance in case of (a) individual attacks and (b) collective attacks for homodyne detection in fog.

Comparing Figs. 7 and 6 shows that, in the case of collective attacks, CVQKD signals employ homodyne detection can transmit farther than that of heterodyne detection under conditions that uses the same wavelength. But in the case of individual attacks, the propagation distance of heterodyne detection is farther than that of the homodyne detection under the same conditions. Therefore, in the practical application, Bob should select an appropriate detection mean based on the type of attack the Eve is conducting.

The demonstration of the above theoretical model and corresponding analysis is also suitable for other types of weather conditions, and the SKR is calculated under the same conditions as those used above, except for assuming the signals are transmitted in the fog. The results summarized in Figs. 8 and 9 show that the interruption probability P has little effect on the performance of the quantum communication system in the presence of fog. As expected, the achievable transmission distance is much smaller in fog compared to that in clear weather condition.

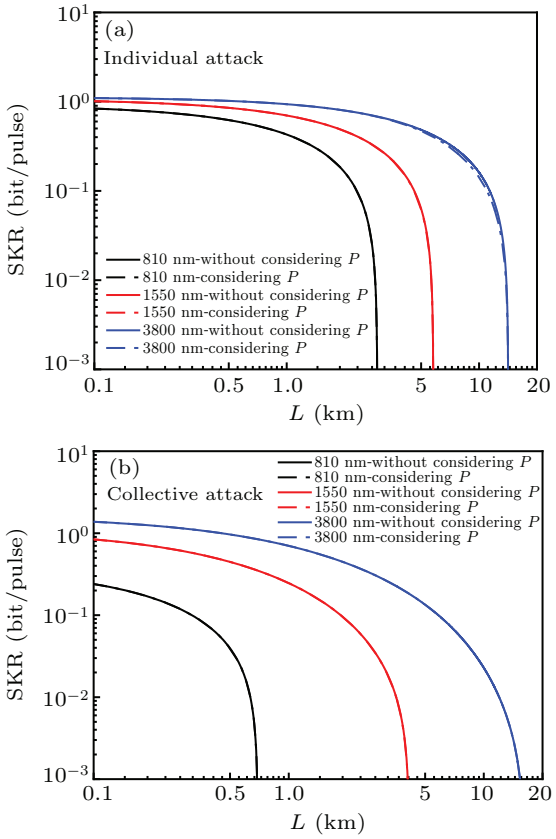


Fig. 9. Relationship between SKR and distance in case of (a) individual attacks and (b) collective attacks for heterodyne detection in fog.

5. Concluding remarks

This paper presents a study on how SKR in CVQKD get affected by the attenuation, excess noise, and interruption probability caused by the atmospheric effects at 810 nm, 1550 nm, and 3800 nm wavelengths, by using either homodyne or heterodyne detection schemes, under individual attacks and collective attacks, in clear weather and fog. An FSO CVQKD transmission model has been established firstly. Then, the transmittance, excess noise and interruption probability have been calculated for 810 nm, 1550 nm, and 3800 nm signal wavelengths. An equation has been given and utilized in the calculation of the interruption probability based on the Kolmogorov spectrum model. We carried out a detailed analysis of the transmittance effects, excess noise, and interruption probability on the SKR. The SKR results indicate that the longest wavelength under study (3800 nm) we can obtain a higher SKR than that of shorter wavelengths for the same propagation distance. Observed differently, for a given SKR much longer transmission distance can be achieved at 3800 nm. On the other, the interruption probability effect appears to be slightly higher at longer wavelengths. Because the interruption probability reduces the SKR at any wavelength, the beam tracking system should be used to solve for this problem. Moreover, when Eve applies the collective attacks and for the same wavelength, a system employing homodyne detection can achieve longer distance than corresponding system using the heterodyne detection. However, this behavior has been reversed when Eve applies the individual attacks. Similar conclusions have been found for clear weather and fog. To conclude, in a practical application, longer wavelengths should be used, such as 3800 nm, given that longer transmission distances can be achieved for the same SKR. However, Bob should select an appropriate detection scheme based on the type of the attack conducted by Eve.

Acknowledgements

Project supported by the National Natural Science Foundation of China (Grant No. 62071180) and Fundamental Research Funds for the Central Universities, China (Grant No. 2020MS099).

References

[1] Miao E L, Han Z F, Gong S S, Zhang T, Diao D S and Guo G C 2005 *New J. Phys.* **7** 215
[2] Peng C Z, Yang T, Bao X H, Zhang J, Jin X M, Feng F Y, Yang B, Yang J, Yin J, Zhang Q, Li N, Tian B L and Pan J W 2005 *Phys. Rev. Lett.* **94** 150501
[3] Raj A, Selvi J and Durairaj S 2015 *Appl. Opt.* **54** 802
[4] Cui X Z, Yin X L, Chang H, Zhang Z C, Wang Y J and Wu G H 2017 *Chin. Phys. B* **26** 114207
[5] Andrews L C and Phillips R L 2005 *Laser Beam Propagation through Random Media* (2nd edn.)(Washingon: SPIE PRESS) pp. 1–783
[6] Fante R L 1980 *Proc. IEEE* **68** 1424
[7] Barbier P R, Rush D W, Plett M L and Polak-Dingels P 1998 *SPIE's International Symposium on Optical Science, Engineering, and Instrumentation*, October 20, 1998, San Diego,CA, United States, 93
[8] Vasylyev D, Semenov A A and Vogel W 2019 *Int. J. Theor. Phys.* **58** 3746
[9] Chai G, Liang K X, Liu W Q, Huang P, Cao Z W and Zeng G H 2019 *Int. J. Theor. Phys.* **58** 3746)
[10] Zhao W, Liao Q, Huang D and Guo Y 2019 *Quantum. Inf. Proc.* **18** 39
[11] Wang S Y, Huang P, Wang T and Zeng G H 2018 *New. J. Phys.* **20** 083037
[12] Mahlobogwane Z, Owolawi P A and Sokoya O 2018 2018 *International Conference on Advances in Big Data, Computing and Data Communication Systems (icABCD)*, August 6–7, 2018, Durban, South Africa, p. 1
[13] Liu T, Zhang J Z, Lei Y X, Zhang R X and Sun J F 2019 *J. Mod. Opt.* **66** 986
[14] Xu J C, Zhang Y X, Wang J Y and Jia J J 2011 *Optik* **122** 586
[15] Hughes R J and Nordholt J E 2017 *Nat. Photon.* **11** 456
[16] Liao S K, Yong H L, Liu C, *et al.* 2017 *Nat. Photon.* **11** 509
[17] Büchter K F, Herrmann H, Langrock C, Fejer M M and Sohler W 2009 *Opt. Lett.* **34** 470
[18] Miguel N and Antonio A 2005 *Phys. Rev. Lett.* **94** 020505
[19] Lodewyck J, Bloch M, García-Patrón R, Fossier S, Karpov E, Diamanti E, Debuisschert T, Cerf N J, Tualle-Brouri R, McLaughlin S W and Grangier P 2007 *Phys. Rev. A* **76** 042305
[20] Qu Z and Djordjevic I B 2018 *IEEE. Photon. J.* **10** 1943
[21] Liu W Q, Peng J Y, Huang P, Huang D and Zeng G H 2017 *Opt. Express* **25** 19429
[22] Huang B, Huang Y M and Peng Z M 2019 *Opt. Express* **27** 20621
[23] Djordjevic I B 2019 *IEEE. Access* **5** 147399
[24] Ricklin J C, Hammel S M, Eaton F D and Lachinova S 2006 *J. Opt.Fiber Commun. Rep.* **3** 111
[25] Kim I I, Mcarthur B and Korevaar E J 2001 *Proc. SPIE* 4214
[26] Qi B, Lougovski P, Pooser R, Grice W and Bobrek M 2015 *Phys. Rev. X* **5** 041009
[27] Liorni C, Kampermann H and Bruss D 2019 *New J. Phys.* **21** 093055
[28] Bedington R, Arrazola J M and Ling A 2017 *Npj. Quantum. Inform.* **3** 30